Structures and Bonding Nature of Small Monoligated Copper Clusters ($HCN-Cu_n$, $n = 1-3$) through High-Resolution Infrared Spectroscopy and Theory

Paul L. Stiles* and Roger E. Miller†

Department of Chemistry, University of North Carolina, Chapel Hill, North Carolina 27599

Received: May 24, 2006; In Final Form: July 4, 2006

The structures, C−H stretching frequencies, and dipole moments of $HCN-Cu_n$ ($n = 1-3$) clusters are determined through high-resolution infrared spectroscopy. The complexes are formed and probed within superfluid helium droplets, whereby the helium droplet beam is passed over a resistively heated crucible containing copper shot and then through a gas HCN pickup cell. All complexes are found to be bound to the nitrogen end of the HCN molecule and on the "atop site" of the copper cluster. Through the experimental C−H vibrational shifts of $HCN-Cu_n$ and ab initio calculations, it was found that the HCN−metal interaction changes from a strong van der Waals bond in $n = 1$ to a partially covalent bond in $HCN-Cu_3$. Comparisons with existing infrared data on copper surfaces show that the $HCN-Cu_n$ bond must begin to weaken at very large copper cluster sizes, eventually returning to a van der Waals bond in the bulk copper surface case.

Introduction

The study of metal clusters and their interactions with small molecules is motivated, in large part, by the possibility of using these smaller, more computationally manageable, clusters as models for the interactions that take place on bulk metal surfaces.[1−8] It is well-documented, however, that metal clusters, transition metal clusters in particular, have properties that can vary wildly with cluster size and often share no similarities with their bulk counterparts.[4,9] Arguably, the most famous example of this behavior is found in small gold clusters.[10,11] When finely dispersed onto a metal−oxide support, these nanoscale gold particles exhibit a previously unanticipated low-temperature catalytic activity for the combustion, oxidation, reduction, and hydrogenation of numerous molecules.[12] Understanding the fundamental causes for this dramatic size dependence of metal clusters is a major driving force in cluster science.

In this paper we present the high-resolution infrared spectra of $HCN-Cu_n$ ($n = 1-3$). The monoligated copper clusters were formed in superfluid helium droplets, which are at a temperature of 0.4 K. The use of superfluid helium droplets as a "nanoscale laboratory" has been well demonstrated in the past decade.[13−17] In one of many applications of this technique, we have shown the particular usefulness of superfluid helium droplets as applied to the study of metal cluster−adsorbate systems.[18,19] One of the unique aspects, and greatest advantages, of helium droplets is that the free rotation of solvated molecules is permitted, due to the weakly interacting nature of the quantum fluid.[20,21] The resulting rotationally resolved spectra, when acquired with use of the appropriate high-resolution spectroscopic techniques, give valuable structural information about the molecular complex solvated with the droplet. Although the rotational constants measured within the droplets are typically reduced by a factor of 2.5 ± 0.5 relative to their gas-phase counterparts,[22−25] the symmetry of the spectra are unaffected.[20]

In addition to structural data, infrared spectroscopy can also provide valuable information about the nature of the interaction between the metal cluster and adsorbate. While many types of spectroscopy have been applied to molecules solvated within helium droplets,[13−17] infrared spectroscopy is particularly well suited, because vibrational transitions are only slightly perturbed (<1 cm^{-1}) from their corresponding gas-phase values.[26] The resulting data can therefore be reliably compared to ab initio calculations and to previous experiments. One such experiment was performed in the laboratory of Michael Trenary at the University of Illinois, Chicago.[27] Celio et al.[27] used both temperature-programmed reaction spectroscopy (TPRS) and reflection absorption infrared spectroscopy (RAIRS) to investigate the properties of HCN on a Cu(100) surface. They found that HCN was weakly bound, nitrogen end down, perpendicular to the copper surface and on an atop site. In this geometry and at temperatures below 90 K, the C−H stretch was measured to be 3294 cm^{-1}. This study was a major inspiration for our choice of copper in the experiments to be presented below. It offers the opportunity to compare the H−CN stretches in clusters [$HCN-Cu_n$ ($n = 1-3$)] and adsorbed on surfaces [HCN−Cu(100)], thus gaining valuable insight into the evolution of the metal cluster−adsorbate interaction as a function of metal cluster size.

Experimental Section

The experimental apparatus has been discussed elsewhere.[28,29] Helium droplets were formed by expanding ultrapure helium through a 5 μm nozzle. The nozzle was cooled to temperatures in the range of 19 to 16 K and backed with 60 bar of helium pressure. These conditions corresponded to average droplet sizes of about 6 000 to 12 000 helium atoms, respectively. After droplet formation and skimming, the droplet beam was passed just over the top of a resistively heated alumina crucible that contained copper shot. Experimental conditions for pickup of one copper atom, on average, required temperatures of about 1130 °C (vapor pressure $= 1 \times 10^{-3}$ Torr), with increasing temperatures for higher order clusters, not exceeding 1250 °C. After the copper pickup, the droplets were then passed through a gas pick up cell containing HCN gas. The pressure inside

* Address correspondence to this author. E-mail: pstiles@unc.edu.
† Deceased.

10.1021/jp063187a CCC: $33.50
Published on Web 08/04/2006

this cell was maintained at pressures below 4×10^{-6} Torr to ensure the pickup of a single HCN molecule/droplet, on average.

The HCN−Cu_n seeded droplets were passed through the laser interaction region, where the C−H stretch of HCN was excited by an F-center laser (Burleigh FCL-20), operating on crystal 3 (RbCl:Li). Subsequent vibrational relaxation to the helium droplet resulted in the evaporation of approximately 600 helium atoms. The depletion of the droplet beam was then detected by a liquid helium cooled bolometer.[30] The laser was amplitude modulated, and the corresponding bolometer signals were measured with phase sensitive detection methods. The details associated with tuning and calibrating the laser can be found elsewhere.[31]

An electric field was applied to the laser interaction region, using two metal electrodes, in order for the acquisition of pendular or Stark spectra. A considerable enhancement of the signal levels was obtained by using a large electric field (∼24 kV/cm) to record pendular spectra,[32,33] which was particularly useful when searching for new unknown species such as those presented here. At more modest electric fields[34] (1−4 kV/cm), the resulting Stark spectra provided accurate measurements of the dipole moments of the HCN−Cu_n complexes.

Results

Computational Details. All MP2 calculations were performed with Molpro.[35] All DFT calculations were performed with Gaussian 03.[36] The relatively large number of electrons associated with copper clusters required the use of effective core potentials (ECP). We chose to use the small core Stuttgart−Dresden ECP (ECP10MDF)[37] due to its familiarity and availability within Molpro. The Stuttgart−Dresden valence basis set for copper [6s,5p,3d] was augmented with 2f functions and a 1g function, as optimized by Martin and Sundermann.[38] The 6-311++G** basis set was used for HCN.

For a better comparison between each cluster, we chose to use restricted open-shell MP2 (ROMP2) methods for HCN−Cu and HCN−Cu_3 as implemented in Molpro. RMP2 methods were used to calculate HCN−Cu_2. It should be noted that with the open-shell systems of HCN−Cu and HCN−Cu_3, restricted open shell MP2 (ROMP2) methods gave much better harmonic frequency results than methods using unrestricted open shell (UMP2). In fact, preliminary calculations that used UMP2 gave large blue-shifts in the C−H stretch frequency for HCN upon complexation with a single copper atom as well as returning unrealistic IR intensities. Given that we were armed with the experimental C−H stretch in the HCN−Cu complex, we disregarded the UMP2 calculations and only used the ROMP2 methods for the open-shell frequency calculations.

The abundance of DFT calculations on copper clusters[39−41] prompted us to perform our own DFT calculations on the HCN−Cu_n clusters. DFT methods were also chosen because of the possibility of comparing the calculations reported here with future calculations on larger copper cluster sizes that will almost certainly require the computational savings offered by DFT. The B3LYP functional was used for all cluster calculations along with the same basis sets that were used for the MP2 calculations.

Comparisons of our bare copper calculations with previous work[42−44,47] and direct comparisons with our experimental data led us to believe that our choices for computational methods were sound. Table 1 gives the results of our MP2 calculations (closed shell) on Cu_2, along with previous experiment and theory. There is near-quantitative agreement between our calculated bond length and Bernath's experimentally determined bond length of copper dimer.[42] The calculated frequency is in excellent agreement as well. Looking to the other best calculation available,[43] one can see that we have quantitative agreement with the CASPT2+RC calculation of Pou-Amrigo et al.[43] The near-perfect agreement of our MP2 calculations with experimental results is most likely due to a fortuitous cancelation of errors and should not be taken as evidence for MP2's superiority over other methods. Table 2 compares our bond lengths, bond angles, and frequencies with some previous Cu_3 calculations. Overall, the Jahn−Teller distorted trimer calculated with ROMP2 methods is in excellent agreement with previous work.[44,47]

TABLE 1: The Bond Length (R_e), Harmonic Frequency (ω_e), and Binding Energy (D_e) Are Compared with Previous Work

Cu_2 $^1\Sigma_g^+$	R_e (Å)	ω_e (cm^{-1})	D_e (eV)
RMP2	2.2178	277.01	1.74
exptl[a]	2.2193	266.46	2.08
CASPT2+RC[b]	2.215	276.8	1.97

[a] Reference 42. [b] Reference 43.

TABLE 2: The ROMP2 Bond Length of the Triangle Legs (R_e), Obtuse Angle (θ) of the Triangle, Symmetric Stretch ($\omega_{S.S.}$), Asymmetric Stretch ($\omega_{A.S.}$), and Bend Frequency (ω_{bend}) of the Jahn−Teller Distorted Obtuse Triangle $^2B_2$ Electronic State of Copper Trimer with Previous Results for Comparison

Cu_3	R_e (Å)	θ (deg)	$\omega_{S.S.}$ (cm^{-1})	$\omega_{A.S.}$ (cm^{-1})	ω_{bend} (cm^{-1})
ROMP2	2.271	66.79	271	152	123
BP86-DFT[a]	2.31	68	253	159	107
exptl[b]			245	130	130

[a] Reference 44. [b] References 45 and 46.

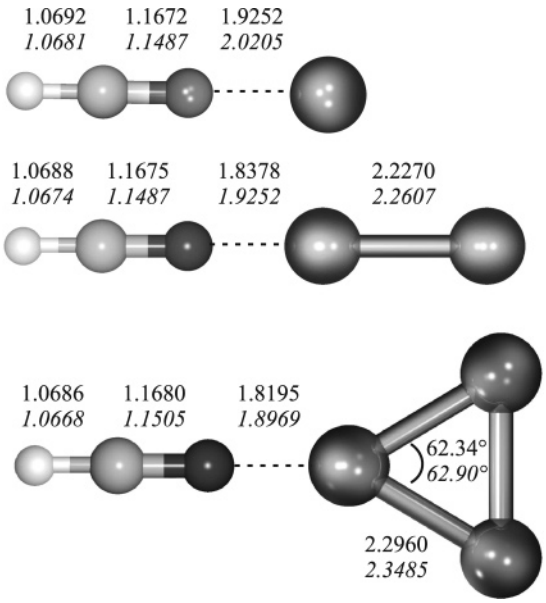

Figure 1. Calculated structures of three HCN−Cu_n complexes. The bond lengths of the MP2 (upper) and DFT (lower) calculations are shown.

The results of our RMP2 and DFT calculations for the HCN−Cu_n clusters are given in Figure 1 and in Table 3. There are no existing calculations on such clusters, but HCN should share many bonding similarities with the widely calculated model ligand, CO. HCN and CO are isoelectronic and both sp hybridized ligands interact with metal clusters through a σ donation mechanism as well as accept charge through the antibonding π orbitals. Fournier[41] has reported the theoretical structures of CO−Cu_n ($n = 1-3$) and compared them to the

TABLE 3: The RMP2 and DFT Harmonic Vibrational Red-Shifts (from HCN monomer), Dipole Moments, and Binding Energy between HCN and Cu_n

	$\Delta\nu$ (cm^{-1})	μ (D)	D_e (kcal/mol)
HCN−Cu			
ROMP2	11.64	7.957	1.73
B3LYP	17.28	5.941	2.92
HCN−Cu_2			
RMP2	7.28	6.322	16.2
B3LYP	5.95	6.323	14.4
HCN−Cu_3			
ROMP2	6.14	6.780	23.1
B3LYP	4.99	5.760	20.6

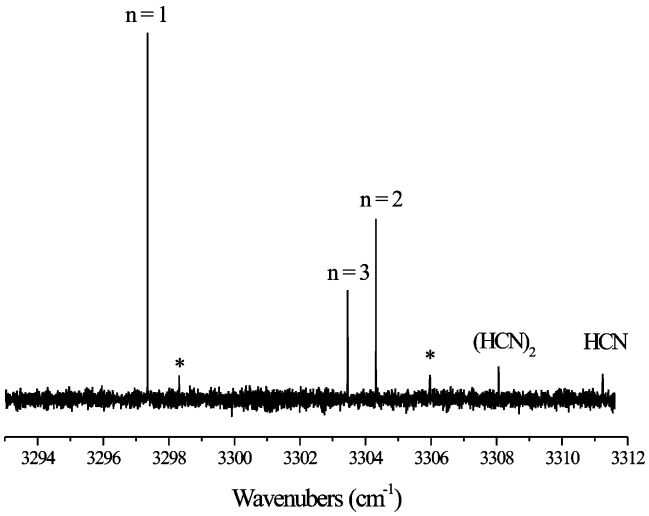

Figure 2. Pendular survey scan of the free C−H stretch region of HCN in the presence of copper. The bands assigned to the three HCN−Cu_n complexes are labeled. The asterisks designate species due to higher order HCN clusters bound to copper.

available matrix isolation infrared data.[48] Our global minimum structures are all consistent with these previous studies.

Pendular Spectrum. We begin the presentation of our experimental results with a long pendular survey scan of the free stretch region of HCN (Figure 2). The laser polarization was oriented so that the electric field component of the light was parallel to the large DC electric field applied to the laser interaction region, resulting in a collapse of rotational structure to a single peak centered approximately on the vibrational origin of each parallel band. The well-known HCN monomer and dimer pendular peaks[49] are labeled and are extremely weak due to the relatively low HCN pressure used for this scan. The peaks not due solely to HCN multimers were initially assigned with the use of signal optimization techniques and are labeled explicitly in Figure 2. The pickup of dopants within the helium droplet beam is determined by the helium droplet size distribution and the conditions of the pickup cell, both of which are known.[13,17,50−52] Therefore, with the laser fixed at the resonant frequency of a particular pendular transition, we can tune the pick-up cell pressure and oven temperature (metal vapor pressure) to optimize the conditions for forming a particular cluster size, thereby maximizing the associated pendular transition signal intensity. Table 4 gives the optimum oven temperature, optimum average droplet size, and optimum HCN pick-up cell pressure for each of the assigned peaks in Figure 2. The conditions for the optimal signal for HCN are shown for comparison. The relatively large droplet sizes required for the HCN−Cu_n complexes are due primarily to the large bond energy released when the complexes are formed within the droplet. It is important to note that our detection method requires that,

TABLE 4: The Optimal Oven Temperature, Average Droplet Size ($\bar{N}$), and HCN Pressure for the HCN−Cu_n Complexes

	oven temp (°C)	$\bar{N}$	HCN pressure (Torr)
HCN		2300	8.0×10^{-6}
HCN−Cu	1030	5700	3.8×10^{-6}
HCN−Cu_2	1130	7200	3.4×10^{-6}
HCN−Cu_3	1200	12000	2.8×10^{-6}

after the complex has been formed within the droplet, a portion of that droplet must remain for a signal to be detected by the bolometer. For example, the formation of copper dimer from two copper atoms releases about 46 kcal/mol of energy.[53] Additionally, the subsequent complexation energy between Cu_2 and HCN releases another 16 kcal/mol of energy (Table 3). This large energy release results in the evaporation of about 4000 helium atoms from the droplet (assuming 5 cm^{-1} per helium atom),[52] and any droplet below the critical size of about 4000 He atoms will contribute nothing to the phase sensitive bolometric detection method. Notice also in Table 4 that a much lower HCN pressure was required for the optimization of each signal. The low-pressure requirements are due to the fact that larger droplets have larger pick-up cross sections.

In previous work we noted that the C−H frequency red-shifts increased with increasing metal cluster−adsorbate interaction energy.[19,54] Interestingly, here we find that the largest frequency shift is due to the HCN−Cu complex, which has the smallest binding energy (Table 3), while the larger binding energy complexes such as HCN−Cu_2 and HCN−Cu_3 are red-shifted to a lesser degree. This vibrational pattern is inconsistent with what would be expected within Dykstra's theory[55] of vibrational frequency shifts due to hydrogen bonding and hints at a fundamental change in bonding when going from HCN−Cu to HCN−$Cu_{n\geq 2}$. In weakly bound complexes, the magnitude of a red-shift is determined by how the potential along the normal coordinate has been changed. The larger the interaction energy, the greater the red-shift. Therefore, the vibrational red-shift pattern observed in the pendular spectrum (Figure 2) hints that the binding energy between HCN and $Cu_{2,3}$ is no longer within the van der Waals regime, in agreement with the large binding energies reported in Table 3.

HCN−Cu. In addition to the signal optimization methods reported above, definitive spectral assignments as well as direct structural evidence of each complex was obtained through high-resolution infrared spectroscopy. Figure 3 shows the field-free, rotationally resolved IR spectrum of HCN−Cu. The spectrum is that of a linear rotor (no Q-branch). The simulated spectrum shown below the experimental spectrum in Figure 3 was obtained by fitting B (rotational constant) and D (centrifugal distortion constant), in the ground and excited state, of a linear rotor Hamiltonian. The results of the fit are given in Table 5 and are consistent with the calculated structure shown in Figure 1. A constant line width of 0.018 cm^{-1} (fwhm) was used to simulate the spectrum in Figure 3 even though there is clearly some variation in the experimental line width as a function of j (rotational quantum number). This behavior of the line widths has been observed in other systems[56] and has been attributed to the inhomogeneous broadening caused by the droplet size distribution.[57]

As this complex has never been observed in the gas phase, we compare our results with the given theoretical calculations. The experimental ground rotational constant, B'', is reduced by a factor of 2.56 and 2.42 from the MP2 and B3LYP equilibrium B constants, respectively. This reduction factor is typical for molecules solvated within helium and is due to the adiabatic

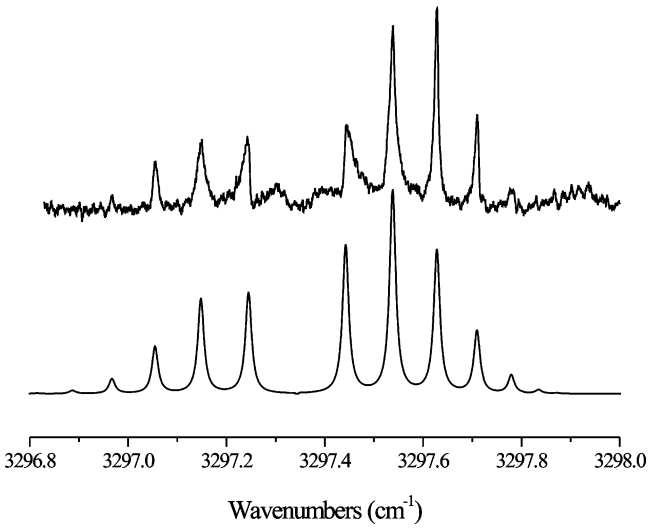

Figure 3. The field free spectrum of HCN−Cu. The simulated spectrum, shown below the experimental one, was fit to a linear rotor Hamiltonian. This spectrum was acquired with an average droplet size of 5700 He atoms.

TABLE 5: The Experimental Vibrational Frequency (ν_0), Vibrational Red-Shift from HCN Monomer ($\Delta\nu_0$), Linear Rotor Rotational Constants (B and D), Dipole Moment (μ), and Line Width (Γ) of HCN−Cu[a]

	exptl		ROMP2	B3LYP
ν_0/cm^{-1}	3297.34			
$\Delta\nu_0$/cm^{-1}	13.9	$\Delta\nu_0$/cm^{-1}	11.64	17.28
B''/cm^{-1}	0.0495	B_e/cm^{-1}	0.1270	0.1201
B'/cm^{-1}	0.0493			
D''/cm^{-1}	9.1×10^{-5}			
D'/cm^{-1}	1.0×10^{-4}			
μ/D	6.40 ± 0.08	μ/D	7.957	5.941
Γ/cm^{-1}	0.018			

[a] The calculated rotational constants, vibrational red-shift (harmonic), and calculated dipole moments are also given. The line width is given at fwhm.

following of helium density surrounding the solvated molecule.[24,58−61] The degree to which the helium density increases the moment of inertia is a very challenging theoretical problem that has been quantitatively resolved for only a handful of small molecules.[14,61−67] Fortunately, many molecules, already know in the gas phase, have been measured in helium droplets and it has been found that the constants are reduced by a factor of 2.5 ± 0.5.[14] The distortion constants, D, given in Table 5 are very large, which is consistent with previous work in helium droplets.[13,14,17]

Although there exists some variation in the line width of each individual ro-vibrational transition in Figure 3, the simulation was generated by using a fixed Lorentizian line width of 0.018 cm^{-1}. Although this line width variation has been observed in previous experiments,[56,68,69] the exact cause of the variation as a function of j is not completely understood, due mainly to the sheer number of possible broadening mechanisms, both inhomogeneous and homogeneous, present within helium droplets.[56] We have acquired several field free spectra of the HCN−Cu complex (not shown) at different average droplet sizes and have observed an increased broadening of the low j states and an increase in the intensity of the broad features between the R(0) and P(1) lines in Figure 3 with decreasing droplet size, suggesting that the broadening is due partly to the inhomogeneous droplet size distribution. The spectra taken at several average droplet sizes also revealed that the unusual line shape of the R(0) and P(1) bands was reproducible and genuine. It is important to note that, due to their asymmetric line shape and ambiguous spectral origin, we ignored the R(0) and P(1) ro-vibrational transitions in the process of fitting the experimental spectrum of HCN−Cu.

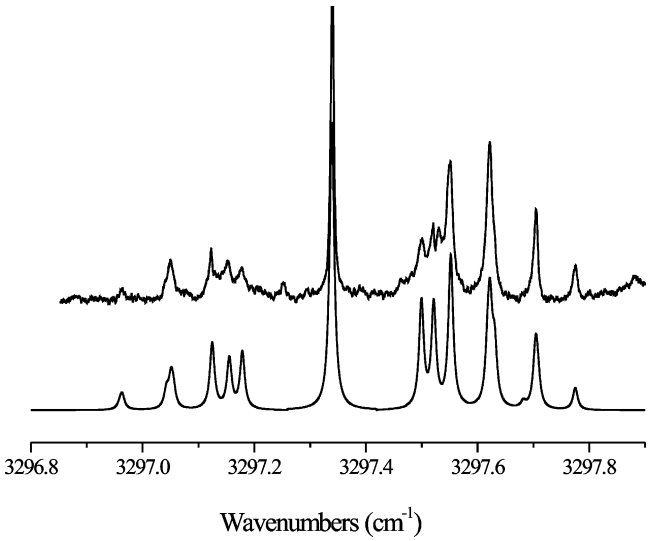

Figure 4. The Stark spectrum of HCN−Cu taken at a field of 1.184 kV/cm.

The Stark spectrum of HCN−Cu is shown in Figure 4. The simulated spectrum shown below the experimental spectrum was generated with our "pendular rotor" program, which diagonalizes the Stark Hamiltonian, using an asymmetric top basis set up to $j = 15$, $m = 12$, and $k = 15$. The previously determined rotational constants were combined with the known electric field present during the spectrum's acquisition, and the dipole moment was adjusted until a good fit was obtained. Several spectra were taken at varying fields with the average dipole moment of all spectra being 6.40 ± 0.08 D. As expected, the experimental dipole moment is somewhat smaller than the ROMP2 dipole moment(6.780 D), which has been explained by the shielding effect the helium solvent has on the electric field experienced by the solvated molecule.[70] The DFT dipole moment (5.760 D) underestimates the dipole moment but, considering DFT's poor performance with weakly bound clusters,[71] this is not surprising.

HCN−Cu_2. Having convincingly assigned the HCN−Cu complex, we now move on to the remaining bands shown in Figure 2. The field free spectrum of the band assigned to HCN−Cu_2 is shown in Figure 5. This spectrum was acquired with a higher copper oven temperature (1150 °C) and a larger average droplet size (7200 He atoms) than the HCN−Cu spectrum, indicative of a complex of larger size. The symmetry of the spectrum gives conclusive evidence that it is due to a linear rotor (no Q-branch), which is consistent with our calculated structure for HCN−Cu_2 (Figure 1).

The experimental spectrum shown in Figure 5 was fitted to a linear rotor Hamiltonian and the rotational constants determined from the fit are given in Table 6. The experimental B'' rotational constant, 0.0178 cm^{-1}, is reduced from the calculated rotational constant (0.03741 cm^{-1}) by a factor of 2.1 and 2.0 for the RMP2 and DFT calculations, respectively. As stated above, this enhancement of the moment of inertia in helium droplets is consistent with previous experiments.

Figure 6 gives the Stark spectrum of HCN−Cu_2 recorded at a 1.05 kV/cm field strength. The result of the fit gave a dipole moment of 6.7 ± 0.3 D. This value is in fair agreement with both the MP2 and DFT theoretical dipole moments, calculated to be 6.322 and 6.323 D, respectively. (Table 6). As was stated

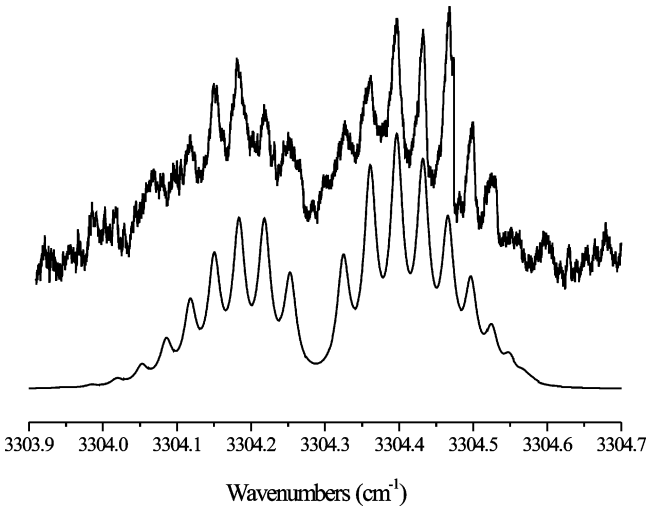

Figure 5. The field free spectrum of HCN−Cu_2. The simulated spectrum, shown below the experimental one, was fit to a linear rotor Hamiltonian. This spectrum was acquired with an average droplet size of 7200 He atoms.

TABLE 6: The Experimental Vibrational Frequency (ν_0), Vibrational Red-Shift from HCN Monomer ($\Delta\nu_0$), Linear Rotor Rotational Constants (B and D), Dipole Moment (μ), and Line Width (Γ) of HCN−Cu_2[a]

	exptl		RMP2	B3LYP
ν_0/cm^{-1}	3304.29			
$\Delta\nu_0$/cm^{-1}	6.92	$\Delta\nu_0$/cm^{-1}	7.28	5.95
B''/cm^{-1}	0.0178	B_e/cm^{-1}	0.03741	0.03601
B'/cm^{-1}	0.0181			
D''/cm^{-1}	8.4×10^{-5}			
D'/cm^{-1}	1.4×10^{-5}			
μ/D	6.7 ± 0.3	μ/D	6.322	6.313
Γ/cm^{-1}	0.02			

[a] The calculated rotational constants, vibrational red-shift (harmonic), and calculated dipole moments are also given. The line width is given at fwhm.

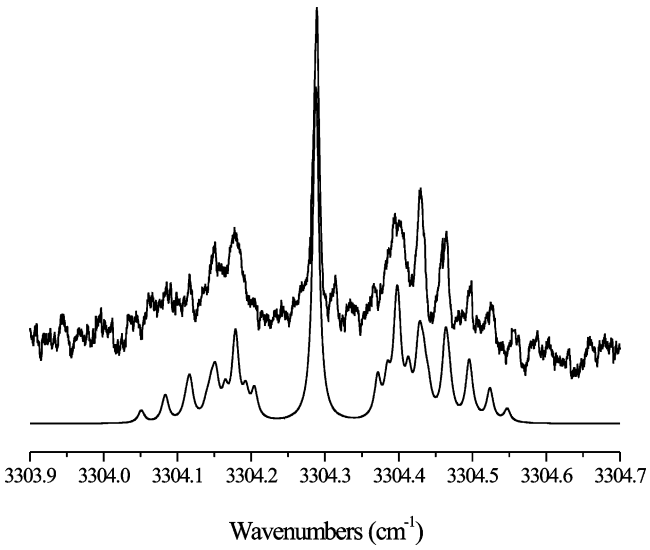

Figure 6. The Stark spectrum of HCN−Cu_2 taken at a field of 1.049 kV/cm.

above, we typically measure slightly smaller dipole moments (1−2%) in helium droplets, due to the shielding effect of the helium solvent.[70] In this case we measure a dipole that is larger than the ab initio and DFT dipole moments. Considering the unambiguous assignment of this band and our confidence in the given Stark spectrum, we attribute the discrepancy to failings in the calculation.

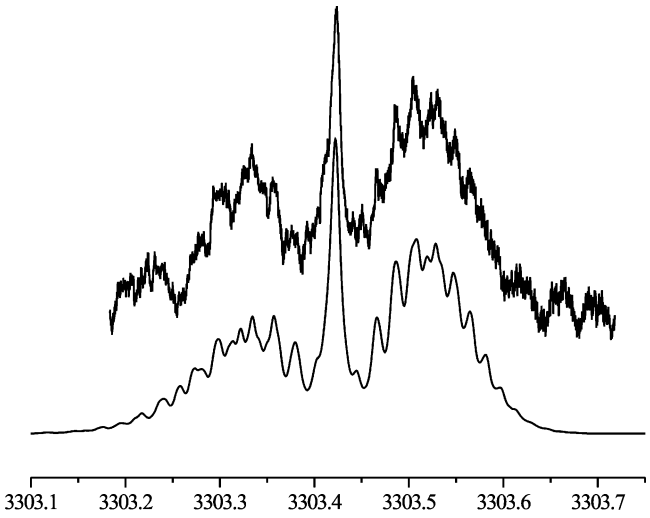

Figure 7. The field free spectrum of HCN−Cu_3. The lower spectrum was generated with use of an asymmetric top Hamiltonian.

TABLE 7: The Experimental Vibrational Frequency (ν_0), Vibrational Red-Shift ($\Delta\nu_0$), Asymmetric Top Rotational Constants Averaged over the Ground and Vibrationally excited states (A, B, C, D_j), Dipole Moment (μ), and Line Width (Γ) of HCN−Cu_3[a]

	exptl		ROMP2	B3LYP
ν_0/cm^{-1}	3303.42			
$\Delta\nu_0$/cm^{-1}	7.79	$\Delta\nu_0$/cm^{-1}	6.14	4.99
$\bar{A}$/cm^{-1}	0.045	A_e/cm^{-1}	0.09347	0.08920
$\bar{B}$/cm^{-1}	0.013	B_e/cm^{-1}	0.03332	0.03207
$\bar{C}$/cm^{-1}	0.0091	C_e/cm^{-1}	0.02456	0.02359
$\bar{D}_j$/cm^{-1}	2×10^{-7}			
μ/D	5.5 ± 0.5	μ/D	6.780	5.764
Γ/cm^{-1}	0.02			

[a] The calculated vibrational red-shift (harmonic), equilibrium rotational constants (A_e, B_e, C_e), and calculated dipole moments are also given.

HCN−Cu_3. The final peak associated with copper and HCN examined in this study is HCN−Cu_3. Its field free spectrum is given in Figure 7. This band optimized at very large average droplet sizes and high oven temperatures (Table 4). The rotational structure of Figure 7 is closely spaced and somewhat unresolved, nevertheless, the overall P-, Q-, and R-branch structure is clearly that of a parallel band of an asymmetric top. The result of the fitting procedure to the A, B, C, and D_j constants of the asymmetric top Hamiltonian is shown below the experimental spectrum. A line width of 0.014 cm^{-1} was used. The collected rotational constants are given in Table 7, and when compared to the calculated values, are all within the expected factor of 2.5 ± 0.5, providing further evidence for the assignment of HCN−Cu_3.

Although the fine rotational structure of the field free spectrum of HCN−Cu_3 is somewhat unresolved, an accurate determination of the rotational constants was still possible through the fitting of the overall shape of the spectrum. This course of action was possible because we have knowledge of the droplet's temperature, namely 0.4 K. Using the resulting rotational constants, the fitting of the overall shape of the Stark spectrum was used to determine the dipole moment of HCN−Cu_3, which is shown in Figure 8. The dipole moment of HCN−Cu_3 was determined to be 5.5 ± 0.5 D. This value is in much

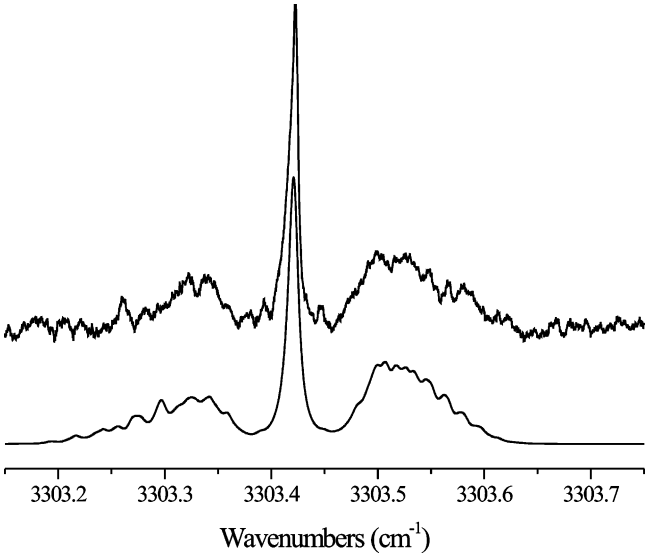

Figure 8. The Stark spectrum of HCN−Cu_3 taken at a field of 1.041 kV/cm.

better agreement with the B3LYP calculated dipole moment (5.764 D) than the ROMP2 dipole moment (6.780 D).

Discussion

The structures of the HCN−Cu_n clusters presented in this report all share a consistent bonding property, namely that the HCN binds to the copper monomer, dimer, and trimer through the nitrogen end of the HCN and on the "atop" site. This similarity in bonding not only offers the opportunity to more easily compare each cluster with one another, but also allows for the meaningful comparison with HCN bound to a Cu(100) surface, since HCN is known to bind (nitrogen end down) to bulk Cu(100) perpendicularly to the surface and at an atop site. As mentioned above, RAIRS and TPRS were used to determine the binding geometry of HCN to Cu(100) at low temperature,[27] so comparisons of the C−H stretching frequency of HCN at the bulk copper limit (3294 cm^{-1}) are possible. In a related theoretical study,[72] the perpendicular binding geometry to the Cu(100) surface was corroborated through DFT calculations of HCN on a Cu_{13} model cluster. The theoretical study also reported the binding energy of HCN on copper as 3.54 kcal/mol and concluded, like Celio and co-workers,[27] that HCN is physisorbed to the copper surface.

It is interesting to note that in our previous[73] and current studies,[74] all of the binary HCN−metal atom complexes were calculated to be bound to the nitrogen in a bent geometry and at large bond lengths, while in the HCN−Cu case, a relatively short, linear bond was calculated. These differences are summarized in Figure 9. The unique geometry for HCN−Cu can be rationalized by examining the van der Waals radii of each metal atom. The copper atom radius (1.40 Å) is much smaller than the Mg (1.73 Å) or Ag (1.72 Å) radii,[75] and as a result, the nitrogen and copper atom can approach more closely. This close proximity permits the donor−acceptor interaction between the nitrogen lone pair and the half-filled 4s copper orbital.[76] The energy of the bond between HCN and Cu remains relatively weak (ROMP2 = 1.73 kcal/mol), due to the balance between the attractive donor−acceptor energy and the repulsive steric interaction.[76] In the case of the Mg and Ag atoms, Pauli repulsion dominates the interaction potential at nitrogen−metal atom distances required for significant charge transfer. In other words, the more diffuse nature of electron density around Mg and Ag prevents significant donor−acceptor interactions from taking place and the atoms are forced to balance their dipole−induced dipole polarization interaction and dispersion interaction by bending closer to the C−N triple bond.

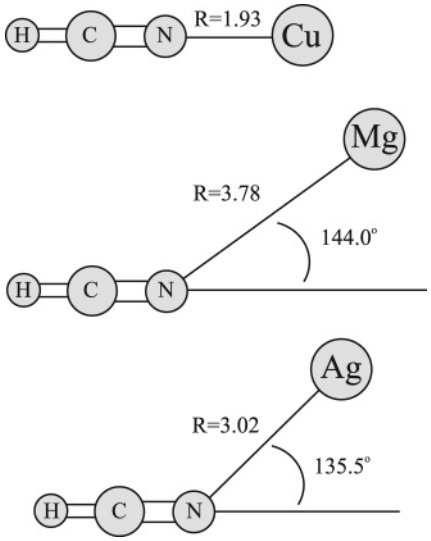

Figure 9. Representative geometries of several HCN−metal complexes calculated with use of MP2 methods.

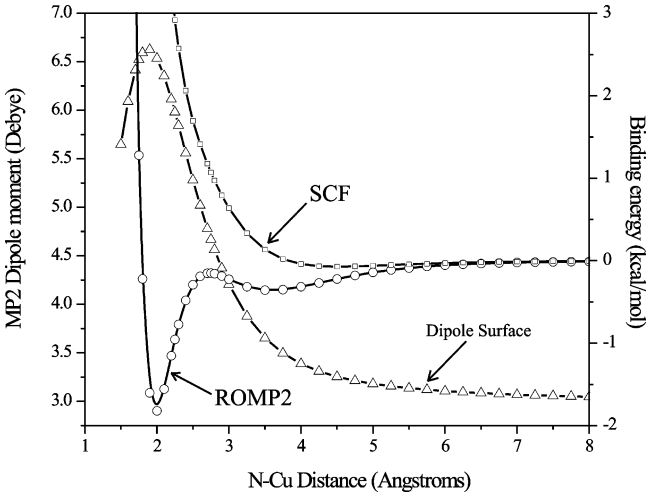

Figure 10. The 1-D SCF and ROMP2 potential energy surfaces of HCN−Cu calculated at distances between the nitrogen on HCN and the nearest Cu atom (see Figure 3). The PES of the SCF and ROMP2 energies are labeled in the plot.

The donor−acceptor viewpoint presented above is consistent with the counterpoise corrected[77] ROMP2 potential energy surface (PES) shown in Figure 10. Coming in from large N−Cu distances, the first shallow minimum is located at about 3.6 Å, distances reminiscent of the HCN−Mg and HCN−Ag bond distances shown in Figure 9. Moving in to shorter distances, the potential rises and peaks at approximately 2.8 Å. It is here that the steric repulsion begins to be overtaken by the attractive charge transfer interaction, caused mainly by the donation of charge from the nitrogen lone pair to the half-filled 4s orbital on Cu. The importance of electron correlation in the HCN−Cu complex is demonstrated by the SCF PES shown in Figure 10, given that there is virtually no binding at the SCF level.

Due to the extremely cold temperature (0.4 K) and rapid cooling capacity of the droplet, the trapping of complexes in local minima on the potential energy surface has been clearly demonstrated in helium droplets.[49,78,79] The dipole moment surface (calculated with the method of finite fields[35]) is therefore

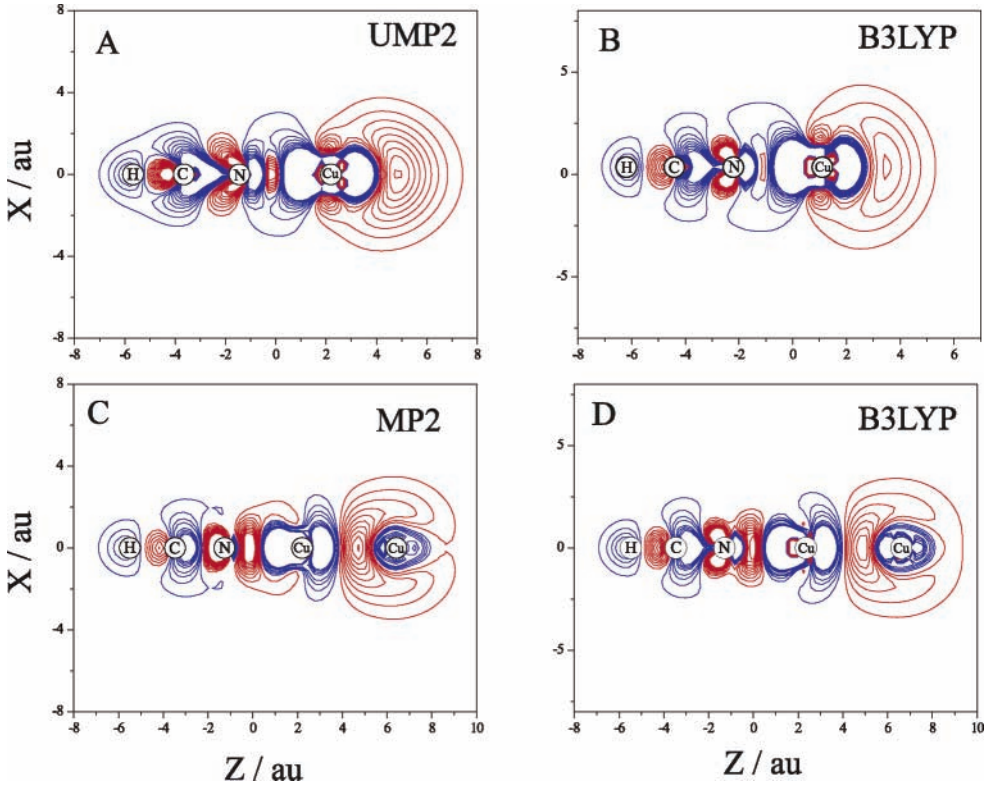

Figure 11. Density difference plots for (A) HCN−Cu with the UMP2 density, (B) HCN−Cu with the DFT density, (C) HCN−Cu_2 with the MP2 density, and (D) HCN−Cu_2 with the DFT density. Contours range from −0.005 to +0.005 e/au^3 and are spaced at 0.0005 e/au^3 intervals. Positive and negative contours are given in red and blue, respectively. ECP and basis set information can be found in the text.

shown along with the PES to further convince the reader that we have indeed captured and measured the ro-vibrational spectrum of the linear structure shown in Figure 9. Consider, for example, the possibility that the HCN−Cu complex was trapped in the shallow minimum at 3.5 Å, shown in Figure 10. The measured dipole moment would be closer to 4.2 D, instead of the measured dipole moment of 6.40 D. This dipole moment is convincing evidence for the reported linear structure.

Although the bonding between HCN and Cu is relatively strong (ROMP2 = 1.73 kcal/mol), compared to binding energies between HCN and other metal atoms (<0.5 kcal/mol), it remains far from the covalent regime. Indeed, the PES shown in Figure 10 predicts virtually no bonding between HCN and Cu at the SCF level.

The physical bond between HCN and Cu is visualized through the use of a difference density plot in Figure 11A,B. ROMP2 densities were unavailable in Molpro so the optimized geometry and densities at the UMP2 level were calculated in Gaussian 03.[36] The electron density difference plot using the DFT density is also given (Figure 11B). Generation of the electron difference density plots involves taking the difference between the electron density of a molecular complex (HCN−Cu) and the densities of a set of noninteracting molecular subunits (HCN and Cu) in the same geometrical arrangement. By looking at the changes in the density between the two cases, one can gain insight into the nature of the intermolecular bonding. In the case of HCN−Cu, Figure 11 clearly shows an overall decrease in the electron density between the nitrogen and copper atom for both the UMP2 and B3LYP densities. This decrease is consistent with a noncovalent interaction, and we conclude that HCN is bound to the copper atom through a strong van der Waals bond.

Much of the interest in metal clusters lies in their ability to change their properties with the addition or subtraction of a single atom. As will be shown below, this is indeed the case

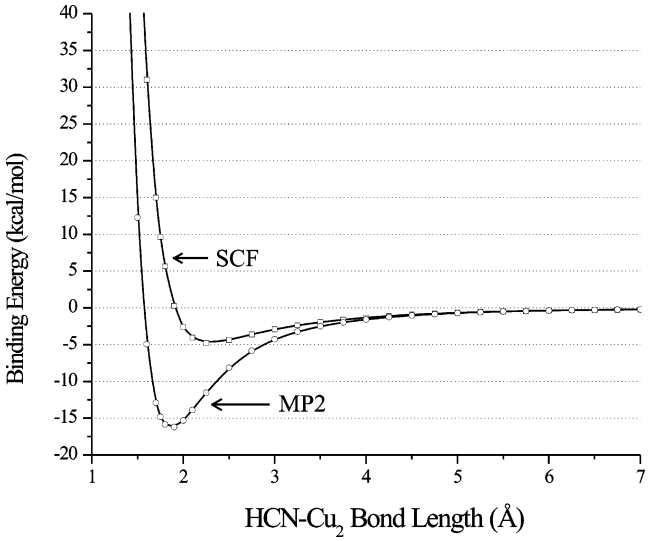

Figure 12. The 1-D SCF and MP2 potential energy surfaces of HCN−Cu_2 calculated at distances between the nitrogen on HCN and the nearest Cu atom (see Figure 3).

when comparing the metal−adsorbate interaction in HCN−Cu_2 and HCN−Cu. Figure 12 shows the 1-D PES of the interaction of HCN and Cu_2. The MP2 PES was calculated at distances between the nitrogen on HCN and the nearest Cu atom on Cu_2 in order for more convenient comparisons among the HCN−Cu_n complexes.

Table 1 gives the equilibrium binding energy of HCN−Cu_2 calculated at the MP2 level (16.2 kcal/mol). The same binding energy is reproduced in the PES given in Figure 12 and represents an extremely large increase in binding energy relative to the binary HCN−Cu complex. What is particularly interesting is the Hartree−Fock PES curve shown along with the MP2

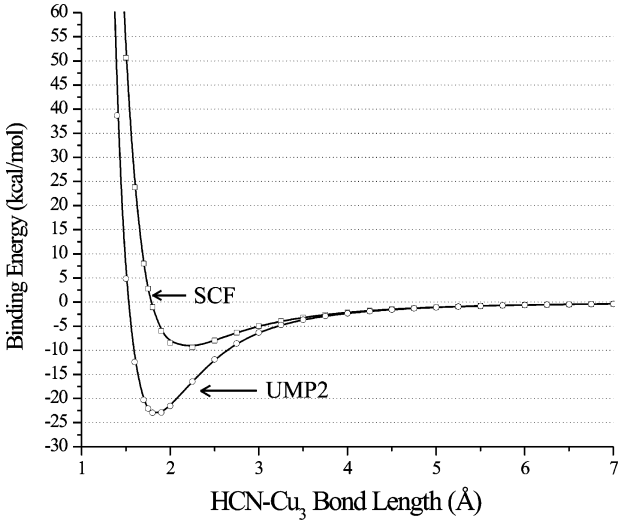

Figure 13. The 1-D SCF and ROMP2 potential energy surface of HCN−Cu_3 calculated at distances between the nitrogen on HCN and the nearest Cu atom (see Figure 3).

surface, which shows just under 5 kcal/mol of binding at a N−Cu distance of 2.25 Å. The significant binding at the SCF level suggests that the interaction between HCN and Cu_2 is not as dependent on electron correlation as what was found for the HCN−Cu complex. Furthermore, it is interesting to note that the total MP2 binding energy is more than 3 times greater than the binding energy of a typical hydrogen bond (5 kcal/mol).

The electron density difference maps of HCN−Cu_2, calculated with MP2 and DFT methods, are given in Figure 11, panels C and D, respectively. The density in both plots is qualitatively different from those calculated for HCN−Cu. In particular, the density contours in the intermolecular bond area between the nitrogen and copper exhibit a large increase in density near the nitrogen, in contrast to the overall decrease in density for the HCN−Cu complex. The polarization of the Cu_2 metal bond is apparent in both the MP2 and DFT density plots and offers a clue to the dramatic increase in binding energy in going from HCN−Cu to HCN−Cu_2.

In 1994, Fournier calculated the bonding of several ligands, including CO, to small Cu_n ($n = 1-3$) clusters, using DFT.[41] In addition to the bonding geometry, Fournier found that the CO−Cu_n clusters share similar binding energies with the HCN−Cu_n complexes reported here. A large increase in binding energy was calculated when going from CO−Cu (19 kcal/mol) to CO−Cu_2 (29 kcal/mol) and it was concluded that this was due to the decrease in Pauli repulsion between CO and the 4s-derived molecular orbital (MO) on Cu_2. The mechanism for this decrease in repulsion was determined to be due to the mixing of the (4s + 4s) σ orbital with the (4s − 4s) σ^* orbital which allows the electron density to polarize away from the CO ligand. Qualitatively, this is what is seen in the electron density difference plot shown in Figure 11C,D. The nodal structure of the (4s − 4s) σ^* is clearly present in the Cu_2 fragment along with the polarization away from the HCN fragment.

We now turn our attention to the HCN−Cu_3 complex and to the PES for this cluster given in Figure 13. This plot shows another large increase in binding energy between HCN and the Cu_3 cluster at both the MP2 and SCF level. The total binding energy has now increased to 23.1 kcal/mol. Like the HCN−Cu_2 complex, the SCF binding suggests that the interaction is fundamentally different from the HCN−Cu case.

The electron density difference plots (UMP2 and DFT) of HCN−Cu_3 are given in Figure 14 and show two views of the planar complex. Panels A and B in Figure 14 give the view of the complex normal to the plane, while panels C and D view the complex in the plane formed by the Cu_3. Before we discuss the features of the density difference plots it is helpful to again revisit the CO−Cu_n calculations of Fournier.[41] Like the CO−Cu_2 cluster, CO−Cu_3 shares some similarities with HCN−Cu_3 that make their comparisons useful. It was determined that the Cu_3 molecular orbitals derived from the in-plane 4p atomic orbitals of Cu, especially those perpendicular to the CO−Cu axis, are the major factors in stabilizing the CO−Cu_3 cluster, compared to the CO−Cu_2 complex. The stabilization energy arises from the mixing of the 4p derived MOs with the π^* MO on CO. Inspecting Figure 14, the importance of the mixing of the Cu_3 MOs with the π^* on HCN is clearly demonstrated. The electron density along the intermolecular bond between the nitrogen and Cu is similar to that of the HCN−Cu_2 complex, while the density *about* the intermolecular axis shows a large increase in density upon complexation, especially in the plane of the Cu_3 clusters (Figure 14A,B). We therefore conclude that HCN−Cu_3, like CO−Cu_3, derives a large part of its binding energy through the mixing of the 4p-derived MOs on Cu_3 and the π^* MOs on HCN.

Having unambiguously assigned each band, we would like to step back from the individual bonding characteristics of each HCN−Cu_n complex and examine the trends in vibrational shifts and binding energy as a function of cluster size. In addition to the complexes presented in this paper, we will also compare the nature of binding and C−H stretching frequency to the bulk copper limit. As was stated above, HCN binds, nitrogen end down, to Cu(100) at an atop site and has a C−H frequency of 3294 cm^{-1}.[27] It was also calculated, using a model Cu_{13} cluster, that HCN binds (nitrogen end down) to an atop site, with a binding energy of 3.54 kcal/mol.[72]

Chemical intuition suggests that the binary HCN−Cu complex, being furthest from the bulk limit, should be the poorest model for the binding of HCN onto a copper surface. However, counter to this intuition, we find that the binary complex is closest to the bulk both in terms of binding energy and in vibrational frequency. The HCN−Cu_2 and HCN-3 are blue-shifted relative to HCN−Cu and also have much higher binding energies. Obviously, at some point in the copper cluster's growth, the C−H stretch and the binding energy between HCN and the copper cluster must reverse the trend and red-shift toward 3294 cm^{-1}, as well as weaken in binding energy.

To investigate the question of when the turnaround in binding energy and frequency shift occurs, we have performed additional DFT calculations on the HCN−Cu_4 complex. The global minimum geometry of HCN−Cu_4 (upper left) and its corresponding electron density difference map (upper right) are given in Figure 15. In these calculations, we used the same DFT methods (B3LYP) and basis sets used for the smaller HCN−Cu_{1-3} clusters. The N−Cu bond length was calculated to be 1.9076 Å, an increase with respect to that of the HCN−Cu_3 but shorter than that of the HCN−Cu_2 complex. This pattern is reflected in the binding energy between HCN and Cu_4 as well. The calculated value of 15.8 kcal/mol lies above HCN−Cu_2 (14.4 kcal/mol) and below HCN−Cu_3 (20.6 kcal/mol). Interestingly, the vibrational frequency red-shift of the C−H stretch from the HCN monomer was calculated to be 1.84 cm^{-1}, showing a continued shift toward higher frequencies with increasing copper cluster size. For completeness, we give the electron density difference plot for HCN−Cu_4 in Figure 15. The pattern of electron density between the nitrogen and nearest copper atom is continued in the HCN−Cu_4 cluster. Similar to

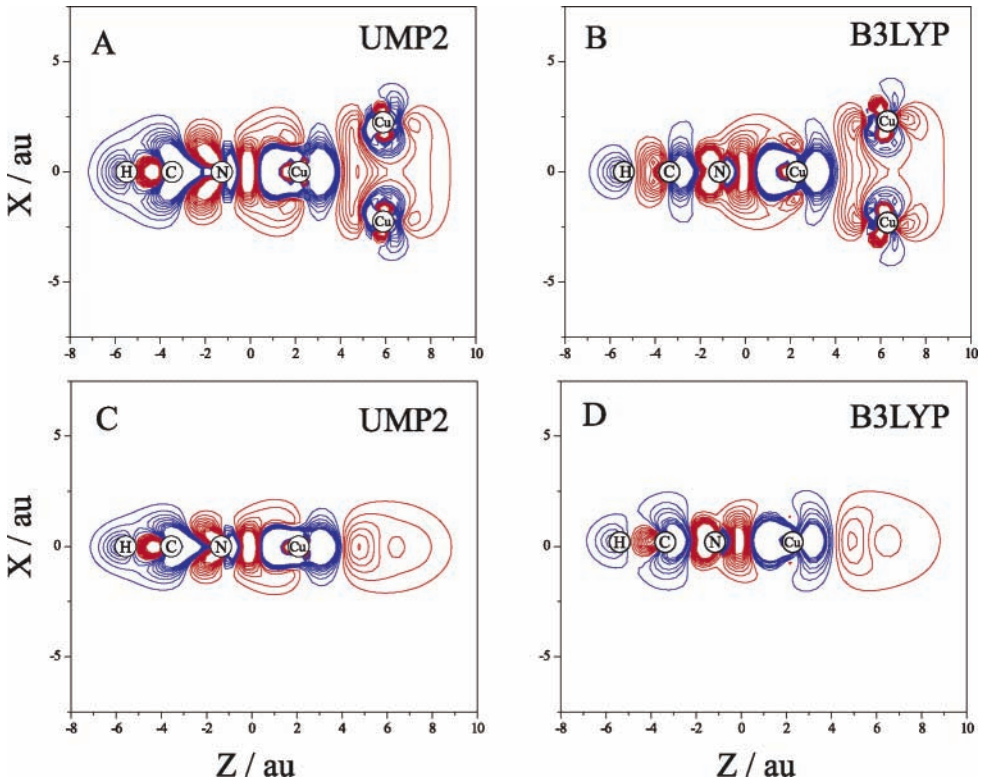

Figure 14. UMP2 and DFT density difference plots for HCN−Cu_3. Panels A and B show the view normal to the Cu_3 plane for the UMP2 and DFT densities, respectively. Panels C and D show the in-plane view of the UMP2 and DFT densities, respectively. Contours range from −0.005 to +0.005 e/au^3 and are spaced at 0.0005 e/au^3 intervals. Positive and negative contours are given in red and blue, respectively.

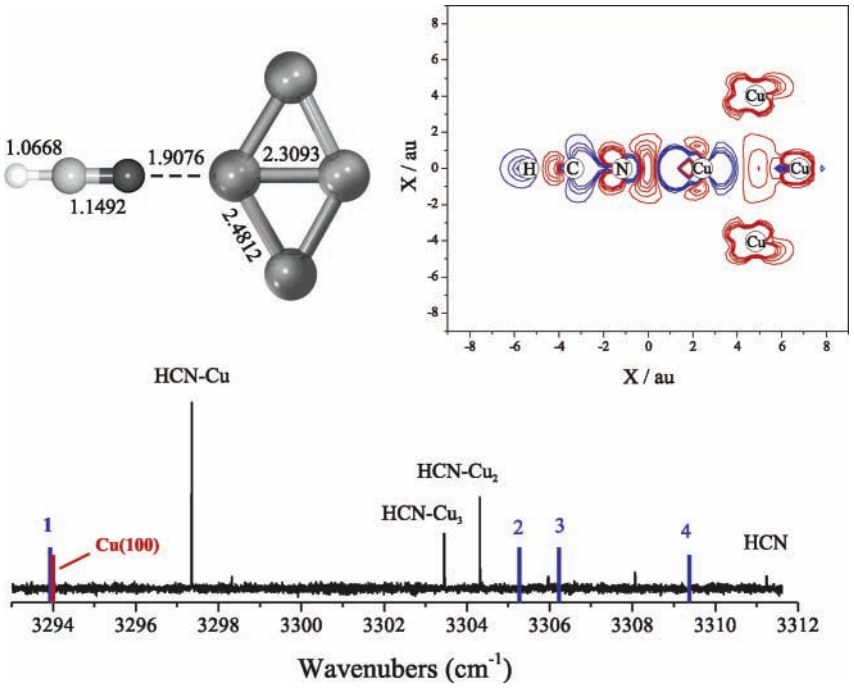

Figure 15. The bond lengths of HCN−Cu_4 (upper left) and the electron density difference plot (upper right) calculated with use of the B3LYP functional are given in the upper left and upper right, respectively. Increases in electron density are represented by red contours while blue contours represent decreases in density. The experimental C−H stretches of HCN−Cu_n are overlayed with the experimental HCN−Cu(100) C−H stretch[27] (red) and the calculated HCN−Cu_n DFT C−H frequencies (blue). The reported DFT frequencies are calculated as frequency shifts from the calculated HCN monomer C−H stretch.

the HCN−Cu_2 and HCN−Cu_3 complexes, there is a large buildup of density near the nitrogen upon complexation, but there also appears to be slightly less density buildup about the N−Cu bond axis, when compared to HCN−Cu_3. This density pattern suggests that charge donation from the 4p MOs on Cu_4 to the π^* orbitals on HCN is less important than what was calculated for the HCN−Cu_3 complex (Figure 14).

A summary of the experimental and DFT vibrational frequencies is shown in the lower area of Figure 15. This plot is given to emphasize the vibrational shift pattern both observed and

calculated for this system. It should be noted that we did not experimentally observe the HCN−Cu_4 complex, which is merely a result of current limitations in experimental methods. The capture of larger metal clusters should be possible by the use of larger helium droplets, which are made possible through the advances in closed-cycle helium refrigerator equipment. Many of these issues are discussed more thoroughly in an upcoming review article.[26]

Assuming that the HCN−Cu_4 calculation is accurate, it is clear that the complex has not yet "turned back" toward the bulk surface regime. We are left with the question: How large must the copper cluster become so that HCN's C−H stretch and binding energy approach the bulk limit? The answer was addressed already by Fournier through his CO−Cu_n theoretical study.[41] We have already discussed similarities in geometry between the CO−Cu_n and HCN−Cu_n complexes. Apparently, there are also similarities in the trend of the binding energy between ligand and metal cluster as the cluster approaches the bulk limit. While discussing the binding energies of each CO−Cu_n cluster, Fournier commented that CO was calculated to be bound to the small copper clusters at energies 10−20 kcal/mol larger than what was measured for CO on a copper surface. Because the binding energy must become smaller at a critical copper cluster size, he speculated that only when clusters become large enough to have flat faces will the interaction energy approach the bulk limit. We feel that this is an excellent interpretation and similarly speculate that HCN will begin to decrease in binding energy and start to shift its C−H stretch back toward 3294 cm^{-1} when the copper cluster becomes large enough to minimize the sharp corners on which the HCN adsorbate preferentially binds.

Summary

The rotationally resolved infrared spectra of HCN−Cu, HCN−Cu_2, and HCN−Cu_3 solvated in helium droplets have been reported. Through the comparisons of theoretical calculations with measured rotational constants, dipole moments, and frequency shifts, we have reached unambiguous structural assignments for each complex. These structures are very similar to theoretical structures reported for CO−Cu_{1-3}.

The frequency shifts and calculated binding energies between HCN and Cu_{1-3} indicate that a dramatic change in the nature of binding occurs with increasing Cu cluster size. The HCN−Cu complex is weakly bound and van der Waals in nature, while the HCN−Cu_2 and HCN−Cu_3 are much more strongly bound and show covalent character in their electron density difference plots. This change in the nature of binding is reflected in the frequency shifts, as the HCN−Cu_2 and HCN−Cu_3 are blue-shifted relative to HCN−Cu, indicating a breakdown in the hydrogen bond model of frequency shifts.[55]

Comparisons of this work with previous RAIRS studies of HCN on a Cu(100) surface suggest that at large enough clusters, the HCN−Cu_n complex will begin to red-shift back toward the bulk limit (3294 cm^{-1}) as well as revert to a weak van der Waals type bond.

Acknowledgment. This work was supported by the NSF (CHE-04-46594). Many thanks to Tomas Baer, Gary Douberly, and Rebecca Wolfe for their critical readings of the manuscript.

References and Notes

(1) Hermann, K.; Witko, M. *J. Mol. Struct.* **1999**, *458*, 81.
(2) Hermann, K.; Witko, M.; Michalak, A. *Z. Phys. Chem.* **1996**, *197*, 219.
(3) Puddephatt, R. J. *Metal Clusters in Catalysis—An Overview*; Wiley-VCH: New York, 1998; Vol. 2.1, pp 605−615.
(4) Moskovits, M., Ed. *Metal Clusters*; Wiley-Interscience: New York, 1986.
(5) Duncan, M. *Int. Rev. Phys. Chem.* **2003**, *22*, 407.
(6) Zakin, M. R.; Brickman, R. O.; Cox, D. M.; Reichmann, K. C.; Trevor, D. J.; Kaldor, A. *J. Chem. Phys.* **1986**, *85*, 1198.
(7) Knickelbein, M. B.; Koretsky, G. M. *J. Phys. Chem. A* **1998**, *102*, 580.
(8) Evans, C.; Gerry, M. C. L. *J. Phys. Chem. A* **2001**, *105*, 9659.
(9) Moskovits, M. *Acc. Chem. Res.* **1979**, *12*, 229.
(10) Haruta, M.; Tsubota, S.; Kobayashi, T.; Kageyama, H.; Genet, M. J.; Delmon, B. *J. Catal.* **1993**, *144*, 175.
(11) Sanchez, A.; Abbet, S.; Heiz, U.; Schneider, W. D.; Hakkinen, H.; Barnett, R. N.; Landman, U. *J. Phys. Chem. A* **1999**, *103*, 9573.
(12) Haruta, M. *Catal. Today* **1997**, *36*, 153.
(13) Toennies, J. P.; Vilesov, A. F. *Annu. Rev. Phys. Chem.* **1998**, *49*, 1.
(14) Callegari, C.; Lehmann, K. K.; Schmied, R.; Scoles, G. *J. Chem. Phys.* **2001**, *115*, 10090.
(15) Northby, J. A. *J. Chem. Phys.* **2001**, *115*, 10065.
(16) Stienkemeier, F.; Vilesov, A. F. *J. Chem. Phys.* **2001**, *115*, 10119.
(17) Toennies, J. P.; Vilesov, A. F. *Angew. Chem., Int. Ed.* **2004**, *43*, 2622.
(18) Nauta, K.; Moore, D. T.; Stiles, P. L.; Miller, R. E. *Science* **2001**, *292*, 481.
(19) Stiles, P. L.; Moore, D. T.; Miller, R. E. *J. Chem. Phys.* **2004**, *121*, 3130.
(20) Hartmann, M.; Miller, R. E.; Toennies, J. P.; Vilesov, A. F. *Phys. Rev. Lett.* **1995**, *75*, 1566.
(21) Barnett, R. N.; Whaley, K. B. *J. Chem. Phys.* **1993**, *99*, 9730.
(22) Kwon, Y.; Ceperley, D. M.; Whaley, K. B. *J. Chem. Phys.* **1996**, *104*, 2341.
(23) Kwon, Y.; Whaley, K. B. *J. Chem. Phys.* **2003**, *119*, 1986.
(24) Kwon, Y.; Whaley, K. B. *Phys. Rev. Lett.* **1999**, *83*, 4108.
(25) Draeger, E. W.; Ceperley, D. M. *Phys. Rev. Lett.* **2003**, *90*, 065301.
(26) Choi, M. Y.; Douberly, G. E.; Falconer, T. M.; Lewis, W. K.; Lindsay, C. M.; Merritt, J. M.; Stiles, P. L.; Miller, R. E. *Int. Rev. Phys. Chem.* **2006**, *25*, 15.
(27) Celio, H.; Mills, P.; Jentz, D.; Pae, Y. I.; Trenary, M. *Langmuir* **1998**, *14*, 1379.
(28) Nauta, K.; Moore, D. T.; Miller, R. E. *Faraday Discuss. Chem. Soc.* **1999**, *113*, 261.
(29) Nauta, K.; Miller, R. E. *J. Chem. Phys.* **1999**, *111*, 3426.
(30) Cavallini, M.; Gallinaro, G.; Scoles, G. *Z. Naturforsch. A* **1967**, *22*, 413.
(31) Huang, Z. S.; Jucks, K. W.; Miller, R. E. *J. Chem. Phys.* **1986**, *85*, 3338.
(32) Rost, J. M.; Grin, J. C.; Friedrich, B.; Herschbach, D. R. *Phys. Rev. Lett.* **1992**, *68*, 1299.
(33) Block, P. A.; Bohac, E. J.; Miller, R. E. *Phys. Rev. Lett.* **1992**, *68*, 1303.
(34) Nauta, K.; Miller, R. E. *Phys. Rev. Lett.* **1999**, *82*, 4480.
(35) Werner, H. J.; Knowles, P. J.; Amos, R. D.; Bernhardsson, A.; Berning, A.; Celani, P.; Cooper, D. L.; Deegan, M. J. O.; Dobbyn, A. J.; Eckert, F.; et al. *Molpro*, 2002.
(36) Frisch, M. J.; Trucks, G. W.; Schlegel, H. B.; Scuseria, G. E.; Robb, M. A.; Cheeseman, J. R.; Montgomery, J. A., Jr.; Vreven, T.; Kudin, K. N.; Burant, J. C.; et al. *Gaussian 03*; Gaussian, Inc.: Wallingford, CT, 2003.
(37) Dolg, M.; Wedig, U.; Stoll, H.; Preuss, H. *J. Chem. Phys.* **1987**, *86*, 866.
(38) Martin, J. M. L.; Sundermann, A. *J. Chem. Phys.* **2001**, *114*, 3408.
(39) Florez, E.; Tiznado, W.; Mondragon, F.; Fuentealba, P. *J. Phys. Chem. A* **2005**, *109*, 7815.
(40) Chan, W. T.; Fournier, R. *Chem. Phys. Lett.* **1999**, *315*, 257.
(41) Fournier, R. *J. Chem. Phys.* **1995**, *102*, 5396.
(42) Ram, R. S.; Jarman, C. N.; Bernath, P. F. *J. Mol. Spectrosc.* **1992**, *156*, 468.
(43) Pou-Amerigo, R.; Merchan, M.; Nebot-Gil, I.; Malmqvist, P. A.; Roos, B. O. *J. Chem. Phys.* **1994**, *101*, 4893.
(44) Papas, B. N.; Schaefer, H. F., III *J. Chem. Phys.* **2005**, *123*, 074321/1.
(45) Rohlfing, E. A.; Valentini, J. J. *Chem. Phys. Lett.* **1986**, *126*, 113.
(46) Koizumi, H.; Sugano, S. *J. Chem. Phys.* **1995**, *102*, 4472.
(47) Berces, A. *Spectrochim. Acta, Part A* **1997**, *53A*, 1257.
(48) Moskovits, M.; Hulse, J. E. *J. Phys. Chem.* **1977**, *81*, 2004.
(49) Nauta, K.; Miller, R. E. *Science* **1999**, *283*, 1895.
(50) Lewerenz, M.; Schilling, B.; Toennies, J. P. *Chem. Phys. Lett.* **1993**, *206*, 381.
(51) Harms, J.; Toennies, J. P.; Dalfovo, F. *Phys. Rev. B* **1998**, *58*, 3341.

(52) Lewerenz, M.; Schilling, B.; Toennies, J. P. *J. Chem. Phys.* **1995**, *102*, 8191.
(53) Lide, D. R., Ed.; *CRC Handbook of Chemistry and Physics*; CRC Press: Boca Raton, FL, 1990; Vol. 71.
(54) Nauta, K.; Miller, R. E. *J. Chem. Phys.* **2001**, *115*, 10138.
(55) Liu, S. Y.; Dykstra, C. E. *J. Phys. Chem.* **1986**, *90*, 3097.
(56) Callegari, C.; Reinhard, I.; Lehmann, K. K.; Scoles, G.; Nauta, K.; Miller, R. E. *J. Chem. Phys.* **2000**, *113*, 4636.
(57) Lehmann, K. K. *Mol. Phys.* **1999**, *97*, 645.
(58) Callegari, C.; Conjusteau, A.; Reinhard, I.; Lehmann, K. K.; Scoles, G.; Dalfovo, F. *Phys. Rev. Lett.* **1999**, *83*, 5058.
(59) Lee, E.; Farrelly, D.; Whaley, K. B. *Phys. Rev. Lett.* **1999**, *83*, 3812.
(60) Tang, J.; McKellar, A. R. W.; Mezzacapo, F.; Moroni, S. *Phys. Rev. Lett.* **2004**, *92*, 145503.
(61) Xu, Y.; Blinov, N.; W. Jäger, Roy, P. *J. Chem. Phys.* **2004**, *124*, 081101.
(62) Kwon, Y.; Huang, P.; Patel, M. V.; Blume, D.; Whaley, K. B. *J. Chem. Phys.* **2000**, *113*, 6469.
(63) Kwon, Y.; Whaley, K. B. *J. Low Temp. Phys.* **2005**, *138*, 253.
(64) Lehmann, K. K.; Callegari, C. *J. Chem. Phys.* **2002**, *117*, 1595.
(65) Maroni, S.; Sarsa, A.; Fantoni, S.; Schmidt, K. E.; Baroni, S. *Phys. Rev. Lett.* **2003**, *90*, 143401.
(66) Paolini, S.; Fantoni, S.; Maroni, S.; Baroni, S. *J. Chem. Phys.* **2005**, *123*, 114306.
(67) Moroni, S.; Blinov, N.; Roy, P. *J. Chem. Phys.* **2004**, *121*, 3577.
(68) Nauta, K.; Miller, R. E. *J. Chem. Phys.* **2001**, *115*, 8384.
(69) Nauta, K.; Miller, R. E. *Chem. Phys. Lett.* **2001**, *350*, 225.
(70) Stiles, P. L.; Nauta, K.; Miller, R. E. *Phys. Rev. Lett.* **2003**, *90*, 135301.
(71) Dkhissi, A.; Alikhani, M. E.; Bouteiller, Y. *J. Mol. Struct.* **1997**, *416*, 1.
(72) Jian-Ming, H.; Yi, L.; Jun-Qian, L.; Yong-Fan, Z. *Acta Chim. Sin.* **2002**, *23*, 181.
(73) Stiles, P. L.; Moore, D. T.; Miller, R. E. *J. Chem. Phys.* **2003**, *118*, 7873.
(74) Stiles, P. L.; Miller, R. E. 2006. In preparation.
(75) Bondi, A. *J. Phys. Chem.* **1964**, *68*, 441.
(76) Badenhoop, J. K.; Weinhold, F. *J. Chem. Phys.* **1997**, *107*, 5406.
(77) Boys, S. F.; Bernardi, F. *Mol. Phys.* **1970**, *194*, 553.
(78) Nauta, K.; Miller, R. E. *The Spectroscopy of Molecules and Unique Clusters in Superofluid Liquid Helium Droplets*; Springer-Verlag: Duesseldorf, Germany, 2001; pp 775−792, ISBN 3540673784.
(79) Nauta, K.; Miller, R. E. *Science* **2000**, *287*, 293.